Chapter 4

New Ligands for Enantioselective Oxidations: N-Heterocyclic Carbenes

4.1 Unselective Ligand Systems for Pd-catalyzed Alcohol Oxidations

In 1977 Blackburn and Schwartz[68] reported the $PdCl_2$/NaOAc-catalyzed aerobic oxidation of secondary alcohols sans copper salts and byproducts (other than water). The reaction proceeds at mild (25-38°C) temperatures under 1 atm O_2, though precipitation of palladium was observed at long reaction times. Since then, organic ligands have been identified which improve various aspects of the reaction. Several are reviewed here (Table 4.1), and any could be considered a starting point in an effort to design enantioselectivity into the unselective process.

The pyridine/$Pd(OAc)_2$ system reported by Uemura et al.[28] extended the substrate scope to include primary and aliphatic alcohols. Reaction rates are also accelerated. Ligand screens by Uemura[28] and also Stoltz[31] and Sigman[32] identified other nitrogenous molecules which ostensibly behave as less efficient analogues of pyridine. Employing triethylamine did result in faster reaction rates at low temperatures[69]. Molecular sieves are included in the reaction mixture and serve to disproportionate (or at least sequester) the primary product hydrogen peroxide, driving the reaction to completion. This element of the protocol has been retained by subsequent catalysts operating in organic solvents.

A water-soluble phenanthroline derivative reported by Sheldon and coworkers[29] removes the

necessity of mixing oxygen and organic solvents, rendering the reaction safer and environmentally friendlier. The large rates observed in this system are likely due to the high temperature and the ability of the polar solvent to abstract anions and create vacancies on Pd.

Table 4.1: Ligand systems for Pd-catalyzed alcohol oxidations

Catalyst	O_2 requirement Solvent	Temperature Base	k_{obs}[1] ($M^{-1}hr^{-1}$)
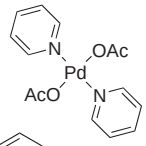	1 atm toluene	80° —	200[2] (benzyl alcohol)
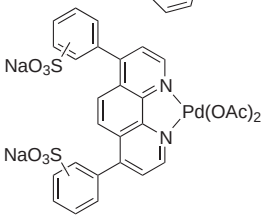	30 atm H_2O	100° NaOAc	>300 (benzyl alcohol) 200 (1-phenylethanol)
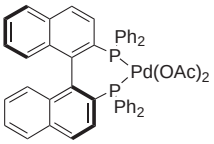	1 atm toluene	80° —	3[3] (1-phenylethanol)
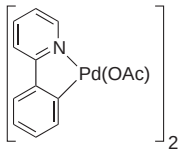	air toluene	80° pyridine	90 (1-phenylethanol)
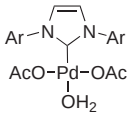	1 atm (air[4]) toluene	50° —	90 (1-phenylethanol) 20[4] (1-phenylethanol)
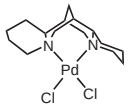	0.2 atm $CHCl_3$	23° $CsCO_3$	5[5] (1-phenylethanol)

[1] Rate constant estimates are based on percent conversion data assuming $-\frac{d[Alcohol]}{dt} = k_{obs}[Pd][Alcohol]$. [2] From reference [30] [3] From reference [31] [4] Excess HOAc inhibits the reaction rate while stabilizing the catalyst against decomposition at low O_2 pressures. [5] From reference [40]

Failing to show enantioselectivity in the screens which identified (–)-sparteine[31, 32], the phosphine (*R*)-BINAP was not studied experimentally in detail. With $Pd(OAc)_2$ it did show activity in the oxidation of 1-phenylethanol, though it is not known whether the ligand itself was simultaneously oxidized under the aerobic conditions. It is mentioned here for the mechanistic questions its activity raises. We predicted, assuming a chelated βHE transtion state geometry like sparteine's,

an observable enantioselectivity ($\mathbf{s}_{calc} = 2$) for a (BINAP)$PdCl_2$ catalyst[1]. Also, formation of a palladium-hydride bond trans to a phosphine ligand is thermodynamically less favorable than trans to an amine or anion (see Figure 3.13). These observations suggest the possibility of an alternative geometry during the C-H_β bond cleavage, perhaps involving the dissociation of one Pd-P bond or the absence of a Pd-H intermediate. Lessons learned from this system might also apply to reactions of palladium carbenes, since, like phosphines, carbene ligands exhibit strong trans effects.

The phenyl-pyridine[70] (and similar phenyl-oxazole[71]) ligand of the Moberg group chelates palladium through a dative Pd-N bond and a covalent Pd-C bond. If this covalent bond is not broken and reformed during every turnover, the activity of this catalyst is the strongest experimental evidence yet that the second half of the catalytic cycle (reoxidation of Pd by O_2) does not require a Pd^0 intermediate. The fact that this catalyst operates under low O_2 pressure (air) without precipitation of palladium black (under normal operating conditions) urges a better understanding of its (perhaps unique) reoxidation mechanism.

Palladium dichloride complexes of chiral and achiral N-heterocyclic carbenes (NHC) were shown by Sigman's group to oxidize 1-phenylethanol enantioselectively when (–)-sparteine was present in solution acting as a chiral deprotonating agent[53]. A more efficient, though unselective, catalyst employs an NHC ligand on palladium diacetate and has recently been described in detail[35, 72]. Rates higher than the (–)-sparteine protocol affords were observed for both benzylic and saturated secondary alcohols. This allows a lower catalyst loading (Pd:substrate ratio of 1:200) than required by kinetic resolutions using ((–)-sparteine)$PdCl_2$ (1:20). The acetate in this system, as in previous systems, serves to deprotonate the alcohol bound to palladium. Excess *acetic acid*, which necessarily drives this deprotonation equilibrium in reverse, was also found to stabilize the catalyst against decomposition at low (ambient) O_2 pressures. It was inferred that the acid reduces the amount of (NHC)Pd^0 present (the likely precursor of Pd black) by simultaneously driving the reaction forward (via protonation of (NHC)Pd(O_2) species) and backward (via oxidative addition of acetic acid) away from (NHC)Pd^0.

[1]The model's anion (chloride) differed from the experiment's, and half the energy difference between the (R) and (S) transition states was due to solvation energy. Together, these may explain the disparity in calculated and observed selectivities without resorting to an alternate transition state geometry.

We chose to pursue the possibility of kinetic resolutions based on the N-heterocyclic carbene platform. Besides the favorable reactivity just described, great synthetic flexibility exists in the construction of NHCs and many C_1- and C_2-symmetric versions are already known (Figure 4.1). One daunting factor to bear in mind is that NHCs proven competent for the reaction of interest are monodentate ligands. Careful consideration was required to identify a ligand whose stereochemistry influences the entire coordination sphere of palladium.

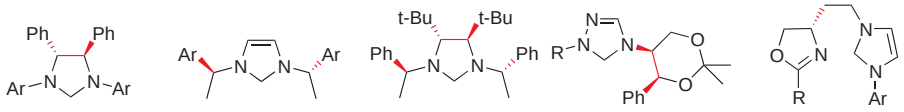

[53] [73] [74] [75] [76]

Figure 4.1: Some known chiral N-heterocyclic carbenes (with references).

4.2 N-Heterocyclic Carbenes

Before a ligand can be designed to perform a kinetic resolution, we must know the geometry of the catalyst-substrate complex at the (intended) moment of enantioselection. Under conditions favorable for both rates and catalyst stability (Pd:HOAc $\approx$ 1:4), C-H_β bond scission appeared be rate-limiting in reactions with (NHC)$Pd(OAc)_2(H_2O)$ as it has for most other catalysts[2]. The next section is therefore dedicated to determining the geometry of the relevant rate-limiting transition state. In the following section we assay the performance of hypothesized ligands assuming enantioselectivities can be predicted using only the relative energies of diasteriomeric transition states (neglecting preceding intermediates involved in pre-equilibria, as with sparteine.)

4.2.1 Mechanism

Another factor which made carbenes a promising scaffold was the quantitative description of the reactivity of **0** ((A)$Pd(OAc)_2(H_2O)$, A = 1,3-bis(2,6-diisopropylphenyl)imidazol-2-ylidene) available in reference [35] and summarized here (Figure 4.2). Correlations between the experimental and calculated data were expected to yield a detailed picture of substrate oxidation, minimizing the need

[2]An exception, the aerobic oxidation of benzylic alcohols by $Pd(OAc)_2$ in DMSO, is limited by the reoxidation of reduced palladium[34].

for assumptions. Two regimes of reactivity were observed: a high acid concentration regime when exogenous acetic acid was added to the reaction mixture (in an acid:**0** ratio greater than ∼3:1) and a low acid regime when no acetic acid was added (other than what is generated in situ by reaction of substrate and **0**). Activation parameters were measured for 1-phenylethanol and benzyl alcohol via Eyring plots between 40 and 55°C. Despite their similar rates in this temperature range, there is a curious discrepancy between the contributions of entropy and enthalpy to the total activation free energy for the two substrates ($\Delta S^{\ddagger}_{1-\text{phenyl}}$ = -3.5 eu, $\Delta S^{\ddagger}_{\text{benzyl}}$ = 12 eu). We note that roughly the same difference in activation entropies was observed between these two substrates using the ((–)-sparteine)$PdCl_2$ catalyst[38]. A first-order dependence of rate on catalyst and 1-phenylethanol concentration was observed under high [HOAc] conditions, while a half-order dependence on substrate concentration was observed in the absence of exogenous acetic acid. The authors also explored the effect of replacing the acetate groups in **0** (along with the excess acetic acid) with carboxylates of varying pK_a. At a acid:**0** ratio of 4:1, the rate of oxidation of 1-phenylethanol increased sharply with the carboxylic acid pK_a: $\log(k_{obs}) = 1.44\ pK_a + C$. In the absence of exogenous acid, this relationship became $\log(k_{obs}) = 0.31\ pK_a + C$.

A notable property of the reaction of **0** with 1-phenylethanol[3] is the unusually high kinetic isotope effect measured when the substrate is deuterated in the β-position. Analogous KIEs measured using ((–)-sparteine)$PdCl_2$ (1.31 [38]), (bathophenanthroline disulfonate)$Pd(OAc)_2$ (1.4 [77]), and $(pyridine)_2Pd(OAc)_2$(1.5[4] [78]) all fell below 2.0. **0** exhibited a KIE of 1.7 when no excess acetic acid was present in solution, but as the acid concentration was increased the measured KIE rose to 5.5 at a Pd:acid ratio of 1:4 without reaching an asymptote. A value of 6.8 was reported earlier for the same catalyst[72]. This observation, along with the monodentate nature of the carbene ligand and its strong trans effect, urged us to consider new mechanistic possibilities beyond those relevant for ((–)-sparteine)PdX_2.

Methods. Reported thermodynamic properties are either solvated energies, E_{sol} (page 13), or enthalpies at 60°C in benzene (Equation 1.1). Electronic energies and optimized structures are

[3] Also observed with 2-decanol.
[4] Measured using β-deuterated benzyl alcohol.

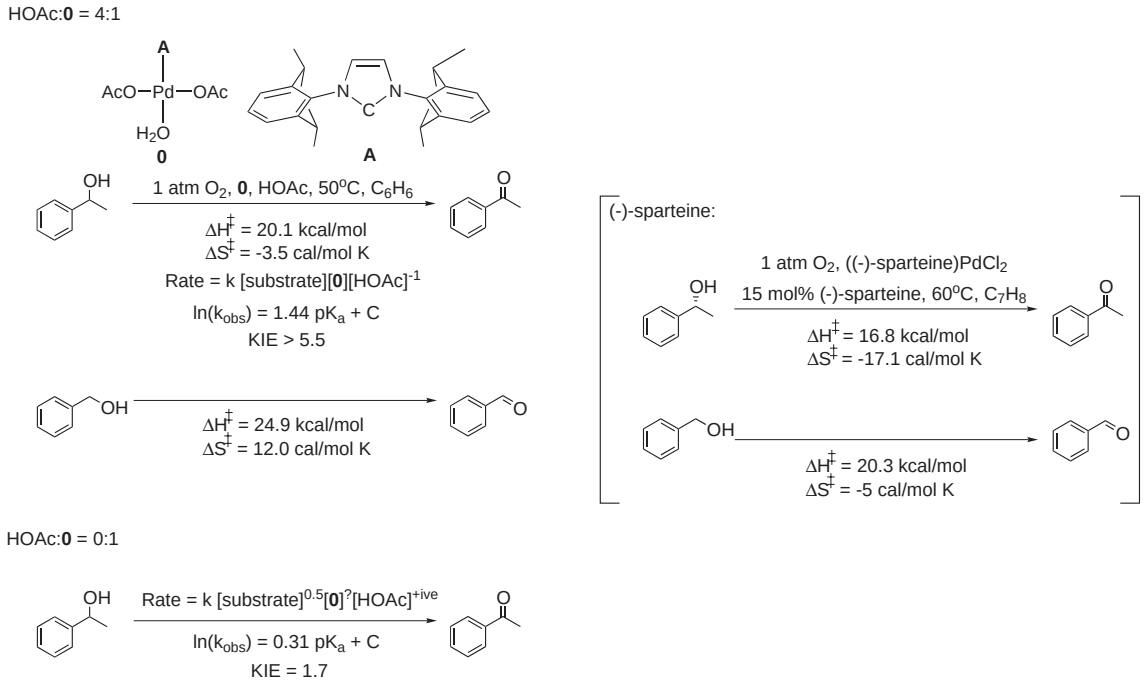

Figure 4.2: Summary of reactivity of (NHC)Pd(OAc)$_2$(H$_2$O), **0**, from reference [35]. (–)-Sparteine data from reference [38].

calculated using the 6-31G**[22, 24] basis set, augmented with diffuse functions on the two active hydrogen atoms, β-carbon, and all oxygen atoms. Hessians used for calculating vibrational spectra and locating transition states were calculated using a smaller basis set, 6-31G, again augmented with polarization and diffuse functions on the listed atoms. Hessian calculations were performed on structures separately optimized using the reduced basis. Palladium was represented with the double-ζ contraction of the LACVP[25] effective core potential and basis set throughout. Solvation energies were computed at gas phase optimized geometries using the polarizable continuum method to represent benzene with $\epsilon = 2.22$ and effective radius 2.6 Å.

When acetic acid leaves the sphere of palladium, it is assumed (for the purposes of calculating relative energies) to exist in solution as hydrogen-bound dimers. The equilibrium constant for dimerization in benzene ($K_{eq} \approx 400$ M^{-1} at 25°C[79]) shows that dimers dominate the population at most acetic acid concentrations, but at the low loadings (0-0.01M) explored by Sigman et al. [35] free monomers are competitive. Even in this case, free water molecules (either preexisting in

the solvent[5], dissociated from **0**, or produced during reaction by the disproportionation of H_2O_2) can stabilize free acid as hydrated monomers[79]. Unreacted substrate molecules (initially present at 0.45M) can also play this role. The calculated enthalpy of dimerization (2 HOAc → $(HOAc)_2$) is ΔH = -9.4 kcal/mol. The calculated enthalpy change for the association of acetic acid and water (H_2O + HOAc → H_2O·HOAc, ΔH = -5.0 kcal/mol) or 1-phenylethanol (C_8H_9OH + HOAc → C_8H_9OH·HOAc, ΔH = -3.9 kcal/mol) coincidentally suggest the same stabilization (within a kcal/mol) per mole acid[6].

Possible C–H_β bond scission transition states. Five geometries for C–H_β bond scission were hypothesized and modeled using 1-phenylethanol as substrate. Comparing thermodynamic and kinetic predictions based on each model to experimental data was expected to identify the correct mechanism. TS1 and TS2 (Figure 4.3) feature traditional β-hydride elimination from a Pd-bound alkoxide, leaving the hydride either cis (TS1) or trans (TS2) to the carbene ligand. Since the strong electron donation of carbene ligands discourages the formation of covalent bonds in the trans position, we also considered the possibility that the β-hydrogen pass directly from the substrate to the free oxygen of a coordinated acetate ligand (TS3). The products of this "reductive" β-hydride elimination are a molecule of acetic acid and a ketone-coordinated Pd^0 complex. In such a mechanism, no intermediates include covalent bonds trans to the carbene.

In TS4 and TS5, the substrate is dehydrogenated in one concerted step. TS4 is analogous to the mechanism of Noyori dehydrogenatation[45] in which the proton-like hydrogen is transferred to a coordinated base (acetate in this case) while the hydride-like hydrogen moves to the metal. To avoid the formation of a palladium hydride, the less traditional TS5 was also considered. Here, both hydrogen atoms are transferred to coordinated acetate groups, again producing acetic acid and Pd^0.

Thermodynamics and kinetics. In examining the thermodynamics of the mechanisms implied by these transition states, the complex (**A**)$Pd(OAc)_2$ (**1**) was chosen as reference, along with free alcohol in solution and O_2 at 1 atm. Sigman et al. [35] showed by NMR that in benzene, the bound

[5]The solubility of water in benzene at 25°C is 0.035M[80, 81]

[6]If the uncomplexed monomer is indeed the most stable state of acetic acid in situ, then the enthalpies of intermediates which have lost HOAc units should be raised by $\frac{1}{2}(9.4) = 4.7$ kcal/mol. The C–H_β bond scission activation enthalpies calculated this way ($\sim$ 23.0 kcal/mol for 1-phenylethanol) are still realistic.

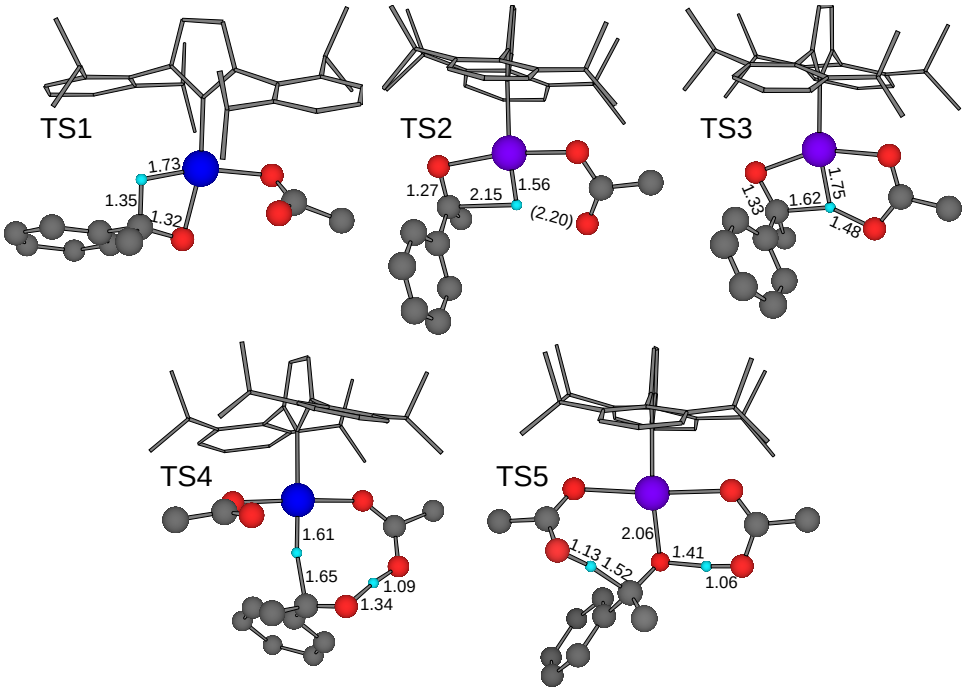

Figure 4.3: C–H_β bond scission transition states modeled. Bond lengths in Å, palladium in blue, oxygen in red, only active hydrogen atoms shown.

water of **0** is dissociated above 0 °C. Relaxation of **1** shows the resulting vacancy is filled by a dative bond from an η^2-acetate anion. Incorporating an explicit solvent molecule showed that the steric crowding around the metal renders a π-adduct (**A**)$Pd(OAc)_2(C_6H_6)$ *less* stable than **1**.

Passage through TS4 does not require prior coordination of the substrate to the catalyst, only the creation of a vacancy. This dehydrogenation path lies 25.7 kcal/mol above state **1** (Figure 4.4).

1-phenylethanol can coordinate to the metal via multiple paths. A low-barrier associative substitution mechanism ($\mathbf{2}^\ddagger$) allows the substrate to displace the dative bond from acetate and coordinate trans to the carbene in **3**. Despite the exothermicity of this substitution, the entropic penalty of immobilizing free substrate is expected to make state **1** dominate the **1**⇌**3** equilibrium. If this were not the case, we would expect a zeroth-order dependence of rate on substrate instead of the observed first-order dependence. TS5 is accessible from **3**, though its calculated enthalpy ($\Delta H^\ddagger$ = 38.2 kcal/mol) shows it is not a viable reaction pathway.

The substrate can also coordinate cis to the carbene by displacing the η^1-coordinated acetate ion. The associative substitution of alcohol for acetate is simultaneous with the deprotonation

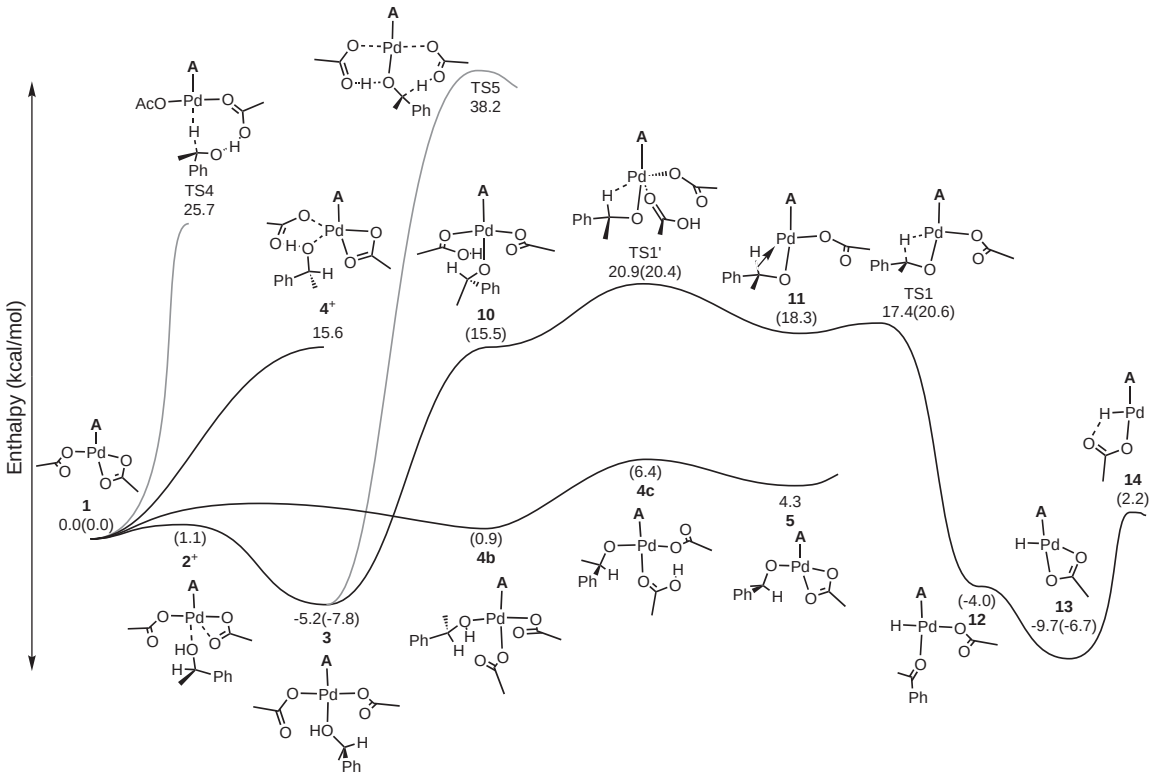

Figure 4.4: Possible mechanisms for the oxidation of 1-phenylethanol by (**A**)Pd(OAc)$_2$. Enthalpies (kcal/mol) at 60°C include solvation by benzene ($\epsilon = 2.22$). Energies (E_{sol}) are given in parentheses since enthalpies were not calculated for all intermediates. Images are projections of the 3D structures.

of the alcohol. The imaginary normal mode of $\mathbf{4}^{\ddagger}$ (with frequency $100i$ cm^{-1}) is composed of the translation of the alcohol and acetate relative to the metal fragment. An intrinsic reaction coordinate (minimum energy pathway) calculation from $\mathbf{4}^{\ddagger}$ confirms that the deprotonation continues exothermically, yielding the Pd-alkoxide **5** after loss of the acetic acid molecule. The barrier to this displacement ($\Delta H^{\ddagger} = 15.6$ kcal/mol) is considerable but not as large as the barriers posed by C–H$_{\beta}$ bond breaking reactions. Attempts to locate a lower-energy, direct transformation of **3** to **5** only led back to $\mathbf{2}^{\ddagger}$.

A lower-energy path for coordinating the substrate cis to the carbene avoids a simultaneous substitution/deprotonation step. Sequential coordination of substrate (**4b**), deprotonation to form **4c**, and dissociation of acetic acid also leads to the alkoxide **5**.

The β-hydride elimination transition state TS1 also has a low enthalpy of $\Delta H^{\ddagger} = 17.4$ kcal/mol. However, we find that no matter how the reactants approach this configuration, it will not provide

the highest barrier of the mechanism. TS1 separates the coordinately unsaturated Pd-alkoxide **11** from the Pd-hydride **12**. This reaction step is so exothermic and the transition state so early that TS1 poses essentially no barrier relative to **11**. (If the Pd-hydride **12** is stabilized by replacing acetate with a more electron-withdrawing carboxylate such as *m*-chlorobenzoate or trifluoroacetate, **11** becomes alltogether unstable and relaxes directly to **12**.) Further reaction of the Pd-hydride **12** via dissociation of the ketone (**13**) and reductive elimination of acetic acid ($\mathbf{14}^{\ddagger}$) is expected to be facile. TS1 is therefore kinetically irrelevant and the rate-limiting step of a mechanism featuring TS1 must fall before **11**.

A low-energy rearrangement of the Pd-alkoxide **5** to form **11** has not been identified, but **11** can be generated by the elimination of acetic acid from state **3**. Transfer of a proton from the bound alcohol to an acetate ligand in **3** yields the Pd-alkoxide **10**. Through the associative substitution TS1′ the bound acetic acid unit is replaced by a β-agostic interaction with the C-H$_\beta$ bond (**11**). The version of TS1 with acetic acid still bound by a hydrogen bond to the remaining acetate ligand (TS1-HOAc) is similar in geometry and enthalpy to TS1. TS1′ is expected to provide the rate-limiting barrier of this pathway, with an activation enthalpy of 20.9 kcal/mol.

The Pd-alkoxide **5** precedes both TS2 and TS3. In the β-hydride elimination step TS2, the oxygen held trans to the carbene is not involved in the reaction after being displaced from the metal. It is also evident from the geometry of TS2 (Figure 4.3) that this is a very late transition state, consistent with the endothermicity of forming a Pd-hydride trans to the carbene ligand in **6**. Intermediate **6** only becomes stable after the Pd-O-C$_\beta$-C$_{\text{phenyl}}$ torsion angle twists such that the O=C$_\beta$ π-orbitals cease to overlap the Pd-H bond. Given the small barrier ($\Delta H^{\ddagger}$ = 3.2 kcal/mol) for the reverse reaction of **6** to TS2, it is doubtful that the reaction can proceed forward from **6** through a transition state with a lower enthalpy than TS2. Dissociation of the ketone from **6** leaves the unsaturated species **7**, while reductive elimination of acetic acid through $\mathbf{8}^{\ddagger}$ poses an overall barrier of $\Delta H^{\ddagger}$ = 22.9 kcal/mol. While greater than the barrier associated with TS3, this value is not far from the observed activation enthalpy of 20.1 kcal/mol. Any reaction through a mechanism including TS2 should be characterized by the reductive elimination step $\mathbf{8}^{\ddagger}$. Since the

stereocenter of the substrate is destroyed before this point, a chiral ligand could not be designed to exert enantioselectivity at this rate-limiting step. The possibility of reaction through $\mathbf{8}^{\ddagger}$ is therefore a critical issue.

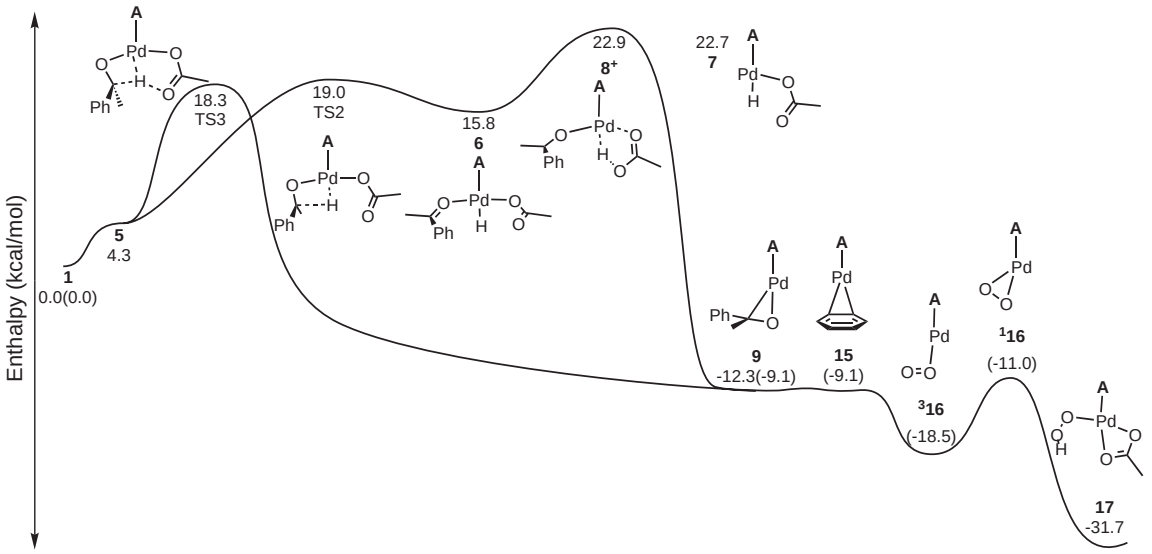

Figure 4.5: Possible mechanisms for the oxidation of 1-phenylethanol by (**A**)Pd(OAc)$_2$. Enthalpies (kcal/mol) at 60°C include solvation by benzene ($\epsilon = 2.22$). Energies (E_{sol}) are given in parentheses since enthalpies were not calculated for all intermediates. Images are projections of the 3D structures.

TS3 combines the β-hydride elimination from the alkoxide with the reductive elimination of acetic acid from palladium in one step. The short Pd-H distance (1.75 Å) in TS3 suggests that the $d_{x^2-y^2}$ orbital lobe trans to the carbene, while unfavorable for hosting the hydride as an intermediate, does stabilize the transit of the hydrogen from carbon to oxygen and accept the two electrons from the C–H$_\beta$ bond. TS3 ($\Delta H^{\ddagger}$ = 18.3 kcal/mol) leads to the (NHC)Pd^0(ketone) complex **9**.

Pd^0 produced by substrate oxidation is expected to exist mainly as the benzene adduct **15**, no less stable than **9**. The interaction of dioxygen and reduced palladium species has been examined recently[51, 82, 49]. Here it is apparent that adsorption of triplet dioxygen on the (NHC)Pd^0 fragment (^{3}**16**) is aided by charge transfer into an antibonding orbital of O_2. A thorough analysis of the catalyst's reoxidation may be given elsewhere; here we note that generation of a hydroperoxide intermediate is exothermic en route to the regenerated diacetate complex **1**. The calculated net reaction enthalpy, assuming a hydrogen peroxide product, is ΔH = -22.8 kcal/mol, but this becomes

-48.4 kcal/mol after disproportionation of the peroxide to free water and dioxygen.

The reactions **5**→TS2→**6** and **5**→TS3→**9** can be represented on the same 2-dimensional potential energy surface (PES) spanned by the C–H_β and H_β–O_{Ac} bond lengths. The PES in Figure 4.6 is constructed from gas phase energies calculated with the augmented 6-31G basis set by constraining these two internal coordinates to different values and allowing all other coordinates to relax. During the reaction through TS2, the H_β–O_{Ac} distance remains large as the C–H_β increases from 1.10 Å in **5** to 3.19 Å in **6**. Note that the gradient of the surface around TS2 is very gentle in both dimensions. The H_β–O_{Ac} distance is not constrained by any bonding interaction, leaving this reaction channel broad perpendicular to the reaction coordinate. The energy profile with respect to the C–H_β coordinate is governed by the formation of the weak Pd–H bond in **6**, so the barrier which must be crossed is very wide parallel to the reaction coordinate as well. The imaginary vibrational frequency calculated at TS2 is only $14i$ cm^{-1}. When Sigman et al. located TS2 they found a C–H_β distance of 1.97 Å, which according to Figure 4.6 implies essentially no difference in activation energy.

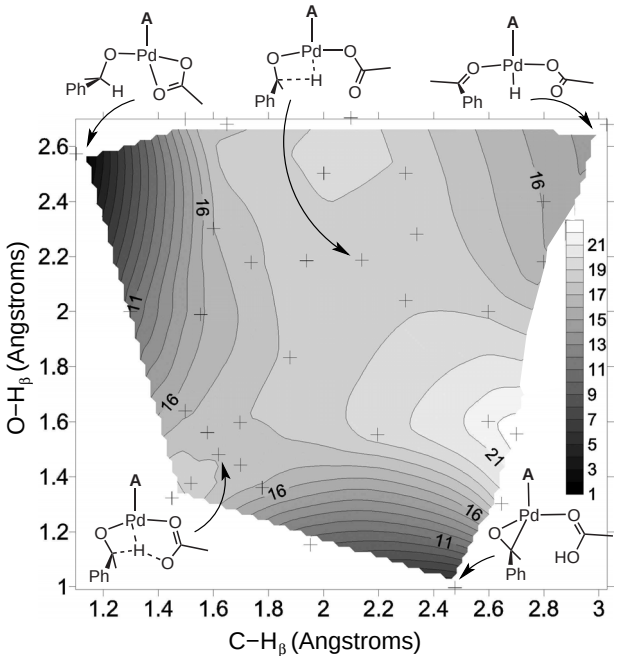

Figure 4.6: Potential energy surface spanned by C–H_β and H_β–O_{Ac} bond distances. Energies (kcal/mol) are gas phase values calculated with the augmented 6-31G basis set (see Methods), relative to the Pd-alkoxide **5**. Plusses mark data points used for interpolation.

On the other hand, the curvature around TS3, both parallel and perpendicular to the reaction coordinate, is pronounced. The energy profile is determined by the formation and breaking of strong C–H and O–H bonds, and the imaginary vibrational frequency at TS3 is $999i$ cm^{-1}.

Thermodynamic properties of key intermediates have been reproduced using benzyl alcohol as substrate in Figure 4.7. The general difference between the substrates is that the calculated enthalpies of intermediates incorporating benzyl alcohol are 1 to 3 kcal/mol more stable relative to state **1**. When measured experimentally, however, benzyl alcohol yielded a *higher* $\Delta H^{\ddagger}$ and lower $\Delta S^{\ddagger}$ than 1-phenylethanol (Figure 4.2). Together, the data suggest that the resting state of the catalytic cycle shifts from **1** when 1-phenylethanol is substrate to $\mathbf{3}_{\text{benzyl}}$ for benzyl alcohol. **1** is calculated to bind benzyl alcohol 3.1 kcal/mol more strongly than 1-phenylethanol. Although the C-H$_\beta$ activation barriers calculated for benzyl alcohol are lower than those for 1-phenylethanol relative to **1**, the measured activation enthalpy in this scenario would be $\Delta H_{\mathbf{3}\rightarrow \text{TS3}} = 24.7$ kcal/mol or $\Delta H_{\mathbf{3}\rightarrow \text{TS1}'} = 24.4$ kcal/mol, in agreement with the experimental value of 24.9 kcal/mol. A shift in resting state also explains the disparate activation entropies: $\Delta S^{\ddagger}_{\text{benzyl}}$ is greater than $\Delta S^{\ddagger}_{1-\text{phenyl}}$ because the unimolecular resting state $\mathbf{3}_{\text{benzyl}}$ has a lower entropy than the bimolecular resting state **1** + 1-phenylethanol. This hypothesis can be easily tested experimentally. If $\mathbf{3}_{\text{benzyl}}$ is indeed the resting state of the cycle at a certain substrate concentration, we expect the reaction rate to be independent of [substrate] at that concentration. A transition to 1$^{\text{st}}$-order dependence on [substrate] would be expected as the substrate concentration was lowered enough to drive the $\mathbf{1} \rightleftharpoons \mathbf{3}_{\text{benzyl}}$ equilibrium back to **1**. Since the ((–)-sparteine)PdCl$_2$ complex was also predicted to bind benzyl alcohol 3 kcal/mol more strongly than 1-phenylethanol, the same shift in resting state could explain the activation parameters measured using that catalyst (Figure 4.2).

Reaction through TS4 and TS5 can be ruled out based only on thermodynamics. In addition to their unrealistic enthalpies (regardless of the resting state of the catalyst), these transition states would have lower entropies than TS2 or TS3, from which a molecule of acetic acid has already been liberated. To within the accuracy of the calculations, the activation enthalpies of TS1′ and TS3 match each other and the measured $\Delta H^{\ddagger}$ of 20.1 kcal/mol, with that of $\mathbf{8}^{\ddagger}$ lying slightly higher. In

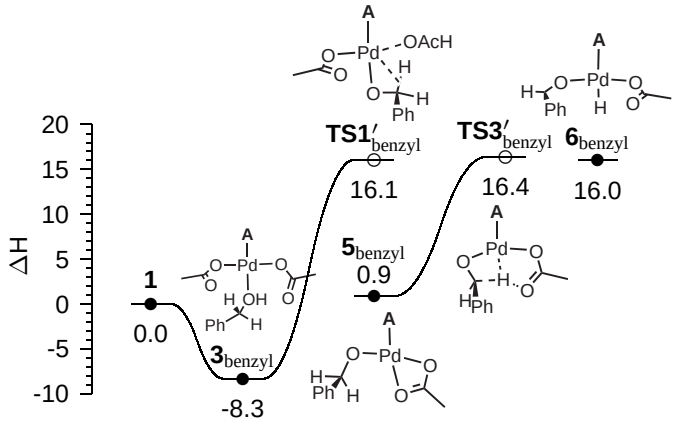

Figure 4.7: Possible intermediates in the oxidation of benzyl alcohol by (**A**)Pd(OAc)$_2$. Enthalpies (kcal/mol) at 60°C include solvation by benzene ($\epsilon = 2.22$).

the following sections, other means of validating one mechanism are sought.

For relating calculated thermodynamics with the observed dependence of rates on isotopic substitution and carboxylate pK_a, rate laws are necessary. For rate laws stemming from paths TS1′, TS2, or TS3, the scheme below is a simple network which can reproduce the reaction orders measured at a high HOAc:Pd ratio[7] (first-order in substrate [R] and total catalyst [Pd]°, inverse first-order in exogenous acid [HOAc]°). If the release and exergonic disproportionation of hydrogen peroxide reaches equilibrium, catalyst states preceding **1** can be ignored. $k_{TS1'}$ is the rate constant for the elementary step **3**→TS1′, while k_{CH} represents whichever step one might consider to be rate limiting among **5**→TS3, **5**→TS2, or **5**→**8**[‡][8].

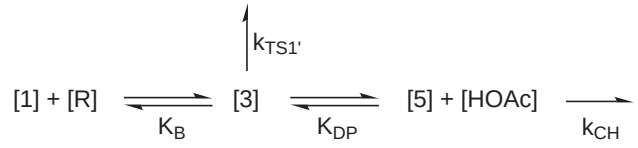

Assuming [Pd]° = [**1**] + [**3**] + [**5**] and [HOAc]° = [HOAc] for conservation of palladium and acid at high acid:Pd ratios, rates limited by $k_{TS1'}$ or k_{CH} can be derived:

$$\text{rate}_{TS1'} = k_{TS1'} K_B [R][Pd]^\circ \tag{4.1}$$

[7]More interesting schemes, involving a palladium-hydroperoxide resting state, can be proposed to explain the complex rate behavior at low [HOAc]°, but this regime offers less insight into the nature of substrate oxidation.

[8]Due to its instability relative to preceding states, accumulation of **6** will be negligible.

and

$$\text{rate}_{\text{CH}} = \frac{k_{\text{CH}} K_{\text{B}} K_{\text{DP}} [\text{R}][\text{Pd}]^{\circ}}{[\text{HOAc}]^{\circ}} \tag{4.2}$$

In each case, state **1** must be assumed the dominant palladium species (i.e., $1 \gg K_{\text{B}}[\text{R}] + K_{\text{B}}K_{\text{DP}}[\text{R}]/[\text{HOAc}]$) to ensure a first-order dependence on [R]. Since no acid is liberated before transition state TS1', this path does not yield the observed inverse dependence on $[\text{HOAc}]^{\circ}$. In itself this argues against the relevance of this route, but equation 4.1 will none the less be used below in arguments regarding KIEs and pK_a dependence. These expressions are consistent with liberated acid molecules existing as lone monomers or water-dimers, but invoking acid-acid or acid-substrate dimers implies unobserved reaction orders. What these expressions confirm is that in either case, the free energy difference on which rates depend is simply the free energy difference between the rate limiting transition state and state **1**. Such a simple relation cannot always be assumed, but the kinetics in this case do not force us to consider more complicated possibilities.

Kinetic isotope effect. For comparison with the anomalous KIE of 5.5 measured using β-deuterated 1-phenylethanol, a kinetic isotope effect was predicted for each of the possible rate-limiting steps considered. In each case, the free substrate is considered the ground state to which the transition state's thermodynamic properties are compared. However, since the vibrational properties of the β-hydrogen are little different in the Pd-alcohol complex **3** and the Pd-alkoxide **5**, KIE predictions made taking either of these states as reference are within half a unit of those shown. "Semi-classical" KIEs were predicted using only the difference in free energies of reaction for the two isotopomers:

$$\text{KIE}_{\text{S-C}} = \frac{k_{\text{H}}}{k_{\text{D}}} = \frac{\frac{kT}{h}\exp(-\frac{\Delta G^{\ddagger}_{\text{H}}}{RT})}{\frac{kT}{h}\exp(-\frac{\Delta G^{\ddagger}_{\text{D}}}{RT})} \tag{4.3}$$

Here $\Delta G^{\ddagger}$ includes the mass-dependent components zero-point energy, internal vibrational enthalpy, and internal vibrational entropy, all evaluated using the appropriately mass-weighted gas phase hessian. Since the transition states under consideration involve the motion of light atoms, we have also considered the likelihood of tunneling contributing to reaction rates and therefore KIEs. Skodje and Truhlar derived an analytical expression (Equation 21 of reference [83]) for approximating the

thermally averaged transmission coefficient κ appropriate for a parabolic barrier. Such a coefficient relates the probabilities of a wave passing over, tunnelling through, or being reflected by a barrier, and can be used to estimate the extent to which a rate calculated by classical transition state theory will be augmented by quantum mechanical tunnelling. Since

$$k_{QM} = \frac{kT}{h}\ \exp(-\frac{\Delta G^{\ddagger}}{RT})\ \kappa\ ,\quad KIE_{QM} = KIE_{S-C}\ \frac{\kappa_H}{\kappa_D} \tag{4.4}$$

The only parameters used in estimating κ are the temperature (50 °C), barrier height (measured from the preceding stable intermediate), and barrier curvature (width). The width of the parabolic barrier is assumed to be related inversely to the imaginary eigenvalue of the mass-weighted hessian. Reducing a highly-dimensional potential energy surface to an isolated one-dimensional parabola along the reaction coordinate is a severe approximation, especially for those segments of the reaction coordinate which are not characterized by the transfer of hydrogen between heavier groups. We therefore are not interested in the quantitative value of the calculated transmission coefficients, but in a qualitative interpretation of the ratio $\frac{\kappa_H}{\kappa_D}$. When this ratio is near unity, the semi-classical KIE will not be enhanced by tunnelling. Because of the exponential decay of wavefunctions under barriers, transmission coefficients (and $\frac{\kappa_H}{\kappa_D}$) will increase suddenly as the height or width of a barrier begins to allow tunnelling. Recall that quantum mechanical penetration of a barrier tends to decrease exponentially with (width)$\sqrt{2(\text{mass})(\text{height})}$; i.e., barrier width is weighted more heavily than height.

Properties of the transition states examined are summarized in Table 4.2 and show a variety of responses to isotopic substitution. In TS1′, the displacement of an acetic acid molecule from Pd by the C-H_β bond, motion along the reaction coordinate involves the entire substrate and acid molecule. Hence, $\nu^{\ddagger}$ is isotope-independent and tunnelling is negligible. The modest KIE of 1.8 belies initial activation of the C-H_β bond, which is elongated to 1.18 Å in TS1′ from 1.10 Å in free 1-phenylethanol.

The β-hydride elimination TS2 on the other hand involves complete C-H_β bond cleavage and is accompanied by a KIE_{S-C} of 3.2. (Mueller et al. calculated a value of 3.8 for the same transition

Table 4.2: Summary of kinetic isotope effect predictions

Transition State	$\nu_{\mathrm{H}}^{\ddagger}(\nu_{\mathrm{D}}^{\ddagger})$ (i cm^{-1})	$\mathrm{KIE}_{\mathrm{S-C}}$	$\kappa_{\mathrm{H}}/\kappa_{\mathrm{D}}$
TS1′	37(37)	1.8	1.00
TS1-HOAc	281(248)	4.0	1.02
TS2	14(14)	3.2	1.00
$\mathbf{8}^{\ddagger}$	666(525)	6.0	1.17
TS3	999(735)	6.2	1.72
TS4	447(430)	3.7	1.01
TS5	1208(947)	4.6	2.53
$\mathbf{4}^{\ddagger}$	100(99)	1.2	1.00

state.) The Pd-H bond has essentially formed in TS2 and the normal mode analysis shows a Pd-H stretch at 1966 cm^{-1} and two orthogonal Pd-H bends[9] around 600 and 800 cm^{-1}. The reductive β-hydride elimination TS3 displays an even higher $\mathrm{KIE}_{\mathrm{S-C}}$ of 6.2 because TS3 loses less zero-point energy upon deuteration. In TS3 the hydrogen is only involved in a Pd-H stretch near 1600 cm^{-1} and a bend at 1014 cm^{-1} orthogonal to translation along the reaction coordinate. Since the two paths have similar activation energies, the tunnelling contribution to each is determined by the barrier thickness. This property is qualitatively illustrated in Figure 4.6 and quantified by the widely disparate imaginary frequencies $\nu^{\ddagger}$ in Table 4.2. Whether the tunneling contribution $\frac{\kappa_{\mathrm{H}}}{\kappa_{\mathrm{D}}}$ is quantitative or not, the reductive β-hydride elimination pathway is capable of exhibiting the large KIE observed experimentally, and perhaps larger if reaction conditions are manipulated to isolate the intrinsic effect.

A catalytic cycle including TS2 is expected to proceed through the reductive elimination of acetic acid in $\mathbf{8}^{\ddagger}$. While TS2 is not predicted to be capable of manifesting the experimentally observed KIE, $\mathbf{8}^{\ddagger}$ is. Since the kinetic properties of the higher (rate-limiting) barrier would be observed, this pathway is therefore also capable of yielding the high KIE measured.

The KIE predicted for the concerted mechanism TS4 is below the experimental value of 5.5. TS5, in which both the active hydrogen atoms of the alcohol are transferred to acetate groups, features a linear $\mathrm{C}\cdots\mathrm{H}_{\beta}\cdots\mathrm{O}_{\mathrm{Ac}}$ geometry which, like TS3, fosters a high $\mathrm{KIE}_{\mathrm{S-C}}$ and high $\nu^{\ddagger}$. Considering the tunnelling effect, this pathway could generate a high kinetic isotope effect, but has already been

[9]It may seem contradictory that there are three hydrogen-dominated modes *in addition* to the imaginary eigenvector $\nu^{\ddagger}$. The motion along the reaction coordinate at TS2 is actually dominated by the ketone, as the O=C bond twists away from the Pd-H bond and a long hydrogen bond forms between a hydrogen on the substrate phenyl group and the free oxygen of the acetate ligand. The flatness of the PES near TS2 and the large mass of the ketone are responsible for the small magnitude of $\nu^{\ddagger}$.

ruled out based on thermodynamics.

These results raise the question of whether the modest KIEs (1.3-1.5) recorded in alcohol oxidations using other palladium catalysts represent C-H$_\beta$ bond scission, formation of a β-agostic interaction, or a convolution of multiple steps.

Rate dependence on pK$_a$. Mueller et al. prepared a series of (**A**)Pd(carboxylate)$_2$(H$_2$O) complexes with carboxylates representing a range of basicity. The rate of 1-phenylethanol oxidation by these catalysts was measured under high acid concentrations, yielding the relation log(k$_{obs}$) = 1.44(±0.13) pK$_a$ + C. Substituting $A_\circ exp(\frac{-\Delta G^\ddagger}{kT})$ for k$_{obs}$ and rearranging yields

$$1.44\mathrm{pK_a} = \frac{-\Delta G^\ddagger}{2.303\mathrm{kT}} + C \tag{4.5}$$

or, at T = 50 °C,

$$\Delta G^\ddagger = -2.13(\pm 0.19)\mathrm{pK_a} + C \tag{4.6}$$

Activation energies have been calculated for possible rate-limiting transition states employing a number of carboxylates. We sought to corroborate or discredit the relevance of proposed pathways by comparing the dependence of their predicted activation energies on pK$_a$ with equation 4.6. To avoid the assumptions associated with using frequencies calculated in the gas phase for solution phase entropies, Table 4.3 reports activation enthalpies and energies. Since electronic effects are responsible for the changes in rate observed here, it is reasonable to expect $\Delta H^\ddagger$ and $\Delta E^\ddagger_{sol}$ to capture the pK$_a$-dependence of rates. The accuracy of solution phase entropy calculations notwithstanding, we note that for TS3 the free energy prediction ($\frac{d(\Delta G^\ddagger)}{d(pK_a)}$ = -1.80) matches the enthalpy prediction ($\frac{d(\Delta H^\ddagger)}{d(pK_a)}$ = -1.74)[10].

Of TS1′, TS2, and TS3, only TS3 is consistent with the strong dependence of rate on basicity. Since both carboxylates of the (**A**)Pd(carboxylate)$_2$ complex have accepted or are accepting protons in this state, it is intuitive that more basic carboxylates will lower the associated activation barrier.

[10]Since the calculated dimerization energies of the carboxylic acids are independent of pK$_a$, the assumption that liberated acid exists as dimers in solution does not affect these relations.

Table 4.3: Dependence of thermodynamic properties[1] on carboxylate pK_a

X-COO^-	acid pK_a	TS1′	**5**	TS3	TS2	**6**	$\mathbf{8}^{\ddagger}$	$\log(k_{obs})$[2]
$(H_3C)_3C$-	5.03	–(–)	–(-0.1)	16.9(20.1)	20.1(23.2)	–(17.6)	–(–)	-3.72
H_3C-	4.76	20.9(20.4)	4.3(2.9)	18.3(21.4)	19.0(21.2)	15.8(16.9)	22.9(27.0)	-4.18
(C_6H_5)-	4.19	20.5(20.8)	–(–)	17.5(20.7)	–(–)	–(–)	–(–)	-4.86
(m-Cl-C_6H_4)-	3.82	–(19.2)	–(2.6)	–(21.4)	–(–)	–(15.8)	–(–)	-5.55
F_3C-	0.3	18.6(19.1)	–(11.5)	25.3(29.3)	20.8(23.9)	–(18.5)	–(–)	–[3]
$\frac{d(\Delta H^{\ddagger})}{d(pK_a)}$	$\left(\frac{d(\Delta E^{\ddagger}_{sol})}{d(pK_a)}\right)$	0.51(0.30)		-1.74(-1.94)	-.25(-.34)		–(–)[4]	

[1] Values are $\Delta H(\Delta E_{sol})$, in kcal/mol, relative to the appropriate (**A**)Pd(carboxylate)$_2$ complex [2] From reference [35], HOAc:Pd = 4:1 [3] Not reported (likely too slow to measure) [4] Not yet available

As noted by the experimentalists, β-hydride elimination barriers are expected to *increase* with carboxylate basicity, since more electron rich anions decrease the electrophilicity of the palladium center. The data do not suggest a clear relationship between the activation energy of TS2 and pK_a.

Activation barriers for the reductive elimination of a carboxylic acid from the catalyst ($\mathbf{8}^{\ddagger}$) are being computed. Given the chemical similarities between state $\mathbf{8}^{\ddagger}$ and state TS3, it will not be surprising to find that the rate of this reaction step is also predicted to match the observed pK_a-dependence.

Finally, recall the relative thermodynamics of the mechanisms containing TS2 and TS3. It is argued (and assumed in the following section) that since the highest barrier posed by the former path ($\Delta H^{\ddagger}$ = 22.9 kcal/mol, $\mathbf{8}^{\ddagger}$) is 4.6 kcal/mol greater than TS3 ($\Delta H^{\ddagger}$ = 18.3 kcal/mol), reaction through TS3 is the dominant mode of substrate oxidation. However, this does not mean that the system does not often pass through TS2 to state **6**, then recross TS2 *unproductively*. Furthermore, we suspect that in state **6**, rotation of the ketone (bound to palladium through oxygen) around the O=C bond axis would be facile. If this rotation were fast enough to equilibrate the *pro*-R and *pro*-S conformations of **6**, this catalyst could racemize an optically pure secondary alcohol independently of any simultaneous oxidation reaction. Of course this process would undermine any attempt to perform a kinetic resolution using a chirally-modified ligand. The occurence of such a racemization could easily be determined experimentally using an enantiomerically pure substrate.

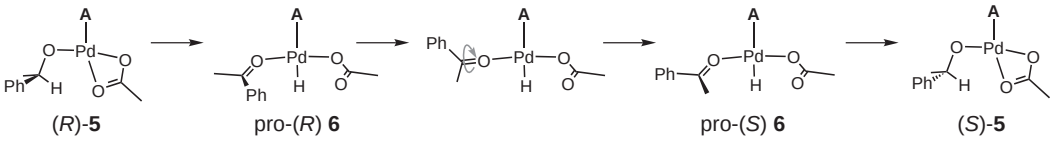

Figure 4.8: Possible mechanism of racemization

4.2.2 Asymmetric Carbenes

Assumptions. Guided by the mechanistic details of the previous section, new chiral carbene ligands were sought which would retain the stability and activity of ligand **A** while introducing enantioselectivity factors typical of the ((–)-sparteine)$PdCl_2$ protocol. It was assumed that enantioselectivities would be determined by the relative energies of rate-limiting, diastereomeric transition states. It is implicit that differences in entropies among such transition states are negligible, though this could be tested directly by comparing internal vibrational entropies calculated after normal mode analyses. Such entropy differences were negligible in the case of (–)-sparteine, but the carbenes considered here feature "loose" rotational degrees of freedom not present in (–)-sparteine. Preceding reaction steps (catalyst reoxidation, binding of substrate by the catalyst, substrate deprotonation) were assumed not to affect reaction rate or selectivity under the acid-rich conditions studied in [35]. Such is the case in kinetic resolutions by ((–)-sparteine)PdX_2[11].

Ligands were screened employing either acetate or pivalate as the carboxylate. Pivalate was shown experimentally to foster a higher reaction rate than acetate[35] and theoretically to yield a lower activation enthalpy for the reductive β-hydride elimination pathway TS3 (above). More critical to a successful kinetic resolution, however, is shutting down reaction pathways which could lead to substrate racemization. The possibility of the reaction sequence (R)-TS2 $\rightarrow$ **6** $\rightarrow$ *equilibration* $\rightarrow$ **6**' $\rightarrow$ (S)-TS2 discussed above must be obviated. A carboxylate with a higher pK_a raises the enthalpy of state TS2 relative to TS3, therefore pivalate is expected to simultaneously foster higher rates and selectivity than acetate. The possibility of extending this effect by substituting tropolone (pK_a = 6.7[84]) for the carboxylic acid was investigated. Calculated thermodynamics employing a simpli-

[11] Although, there is evidence that when (R)- and (S)-1-phenylethanol are oxidized in *separate* reactions (not as a racemic mixture), the relative rates are dependent on the relative stabilities of the diastereomeric Pd-alkoxides formed by the two antipodes[38].

fied carbene (1,3-dimethyl-imidazol-2-ylidene) on palladium ditropolonate suggested that reaction of 1-phenylethanol through either TS2 or TS3 would involve insurmountable barriers ($\Delta H^{\ddagger} > 30$ kcal/mol)[12]. Continued effort will be directed at altering the electronic properties of both anion and ligand to discourage the possibility of unselective reaction through TS2 and $\mathbf{8}^{\ddagger}$.

Methods. Computational parameters similar to those of section 3.1.1 were defined to evaluate the characteristics of hypothetical ligands:

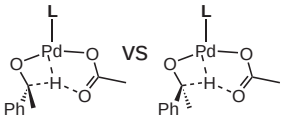

Selectivity

To expidite screening, an iterative approach was taken to the estimation of enantioselectivity. Initially, transition state energies were estimated by freezing the C–H_β and H_β–O distances at the values found in structure TS3 (1.62 Å and 1.48 Å, respectively) and relaxing all other coordinates. The gas phase energies of these structures were combined using equation 2.1 (T = 50°) to generate an estimate, $\mathbf{s}_{\mathrm{froz}-\mathrm{N}}$, where N gives the number of diastereomers modeled. If such a selectivity prediction suggested a ligand deserved further attention, more accurate calculations of the transition states' energies were performed. Partial hessians were constructed for the constrained structures by perturbing the coordinates of the C, H_β, O, and Pd atoms in three orthogonal directions and evaluating forces. Using these hessians, transition state searches were performed in the gas phase and supplemented with single-point solvation energy calculations (in benzene). Selectivities based on these solution phase energies are labeled $\mathbf{s}_{gas-N}$ (denoting the gas-phase transition state optimization). In some cases, transition state searches were performed within the virtual solvent for additional accuracy, yielding a selectivity $\mathbf{s}_{solv-N}$. Selectivities expressed as a fraction denote that (S)-1-phenylethanol is predicted to be the faster reacting enantiomer.

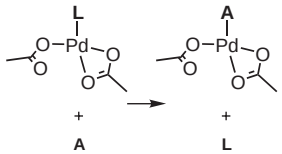

[12]It has not been determined whether this arises from a ground state stabilization of the palladium ditropolonate or an unfavorable positioning of the oxygen lone pair which accepts the β-hydrogen in TS3.

Stability (E_{stable})

The exothermicity of replacing the proposed ligand with the free carbene **A** was used to measure the relative stability of (NHC)Pd$(OAc)_2$ complexes (a positive value denotes improved stability). As with the bispidine ligands of Chapter 3, an acceptable lower bound for this parameter was not known *a priori*. Gas phase reaction energies are given.

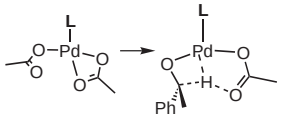

Activation energy (E_{Act})

The difference in energy (electronic plus solvation energy, with no zero-point energy correction) between the diacetate or dipivalate starting material and the lowest-energy diastereomer of the reductive β-hydride elimination transition state incorporating 1-phenylethanol was used as an indicator of reaction rate. For (**A**)Pd$(OAc)_2$, this quantity measured 21.1 kcal/mol.

When studying known catalysts, one purpose of calculations is to quantitatively validate a model against experimental measurements. In this case the accuracy of predictions is paramount. When screening hypothetical catalysts, one is interested in how a new catalyst's properties compare to a known benchmark. In this case, speed takes precedence over accuracy so that a greater variety of candidates can be probed. Accordingly, all calculations in this section use the smaller basis set (the augmented 6-31G/LACVP basis described on page 56), and no zero-point energy or finite-temperature enthalpy or entropy corrections are computed.

Results. As discussed in previous chapters, the principles of volume-exclusion (unfavorable steric interactions) and electrostatics (attractive or repulsive interactions) can be employed to craft a ligand which distinguishes between enantiomeric substrates. These factors were exploited in the ligands below, along with a phenomenon unique to the NHC-Pd^{II} motif. The square plane of palladium prefers to be coplanar with the imidazole plane if the nitrogen substituents of the carbene are not bulky enough to prevent this geometry. Figure 4.9 shows the relative energies of the ground state diacetate complex and transition state TS3, using the sterically simplified ligands 1,3-dihydro- and

1,3-dimethyl-imidazol-2-ylidene. A N-$C_{carbene}$-Pd-O dihedral angle has been constrained to either 0 or 90° in each calculation. The planar structures are lower in energy, especially at the transition state[13]. When the nitrogen substituents on the carbene are aryl groups (as in **A**), the plane of palladium necessarily rotates away from the imidazole plane. This phenomenon can be used to separate the energies of diastereomeric transition states if the nitrogen substituents of the carbene are chosen to allow one enantiomer of the substrate to assume a more planar geometry in TS3.

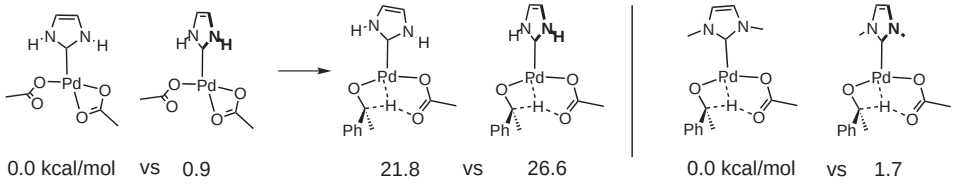

Figure 4.9: Relative energies of structures in which the imidazole and palladium square planes are parallel or perpendicular.

A variety of C_2-symmetric carbenes have been synthesized[73, 74, 85] from chiral diamines which lead to stereocenters at the C_4 and C_5 positions of the imidazole ring (Figure 4.10). Phenyl and t-butyl groups have been introduced in this way, so hypothesized ligands have been limited to these functionalities. Though stereocenters introduced this way are far from other substituents on the metal, chirality propagates to the reaction center through the bulky N-substituents whose conformation is influenced by the C_4- and C_5-substituents. When the N-substituents are aryl derivatives, they twist like propeller blades, forming a C_2-symmetric canopy on one side of the metal atom.

Jensen and Sigman[53] used palladium chloride complexes of ligand **B2** for kinetic resolutions of 1-phenylethanol. With (–)-sparteine present as an exogenous base, selectivity in these reactions (**s** up to 14) was apparently generated during the deprotonation of the Pd-bound alcohol. Similar selectivities were measured whether the C_2-symmetric **B2** or C_{2v}-symmetric carbenes were employed. In the case of palladium diacetate catalysts, C-H_β activation is expected to determine reaction rates and selectivities, and the C_2-symmetric carbenes of type **B** and **C** are not predicted to be capable of inducing satisfactory enantioselectivity (Figure 4.10). Increasing the bulk of the N-substituents from

[13]Whether this is actually caused by electrostatic interaction of the imidazole N–H groups with palladium-bound oxygen or interference between the imidazole π-orbitals and palladium lone pairs is yet to be determined.

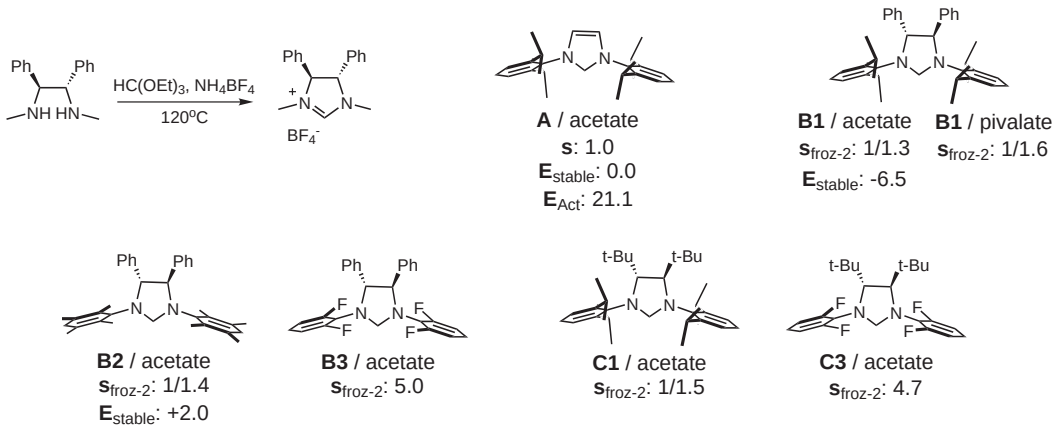

Figure 4.10: C_2-symmetric NHC ligands screened. Synthesis from [85].

2,3,5,6-tetramethylphenyl (**B2**) to 2,6-diisopropylphenyl (**B1**) fails to increase predicted selectivity, though the fluorines of ligands **B3** and **C3** begin to have an effect by directing palladium-bound oxygen atoms in TS3. From such low selectivities it is difficult to discern whether phenyl or t-butyl substituents at the C_4 and C_5 positions are more effective. Stability is predicted to decrease as the bulk of the N-substituents is increased beyond that of planar aryl derivatives.

C_1-symmetric carbenes, in which the N-substituents differ, have been synthesized by multiple routes[86, 87, 76]. Figure 4.11 describes the behavior of several such ligands. Series **D** and **E**, in which one of the large 2,6-diisopropylphenyl groups has been retained, illustrate that the dependence of selectivity on N-substituents is not predictable by inspection. Again, poor selectivities are calculated for candidates of this type, with the notable exception of the adamantyl derivative **F1**. Unfortunately the bulk which effects selectivity in this case renders this ligand less stable than **A**, reminiscent of the bispidines of Chapter 3. Hopes of maintaining the selectivity of **F1** while improving its stability by replacing the adamantyl group with a possibly more flexible t-butyl group proved unfounded (**F3**). In cases where a direct comparison can be made between the selectivities generated by acetate and pivalate complexes (**B1**, **E3** and below), negligible differences are observed. Inspection of the relevant structures shows that the methyl groups of pivalate are located too far from the metal to interfere strongly with the carbene's substituents. In catalysts for which this holds true, the relative enthalpies of states TS2 and TS3 can be modified through the electronic properties of the carboxylate

independently of enantioselectivity. Also fortunate is the prediction that activation energies afforded by the carbenes alkylated at C_4 and C_5 (**E5** and **F1**) are similar to that of **A**.

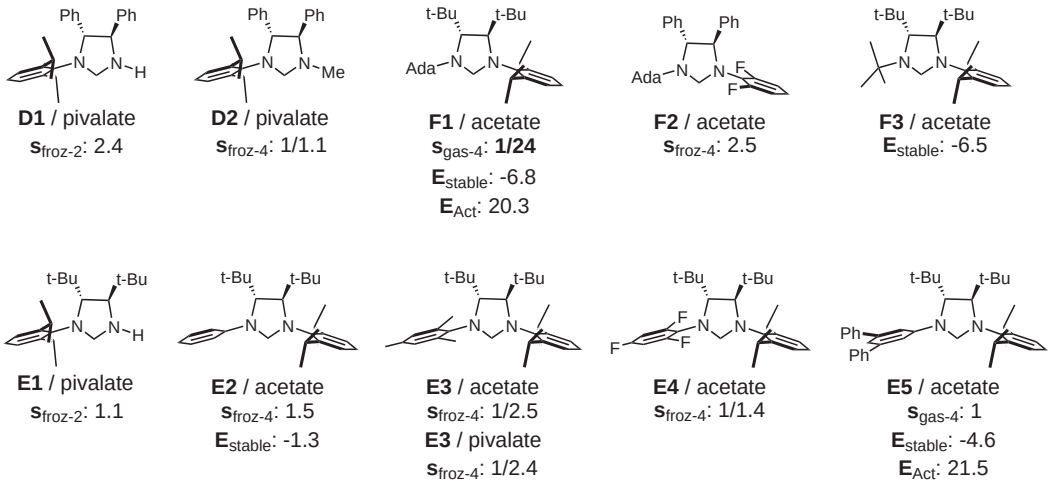

Figure 4.11: C_1-symmetric NHC ligands screened

An unprecedented location for stereocenters was tested in ligands **G** (Figure 4.12). Replacing the isopropyl groups of **A** with optically active chloroethyl groups, a C_2-symmetric environment is again constructed around the metal center. Steric interference between the opposing stereocenters (C*) forbids rotation around the aryl–C* bond. Selectivities generated this way are modest, but more consistent than above. The matched (*R*,*R*) diastereomer **G3**, though promising better selectivity than the unmatched (*R*,*S*) diastereomer **G2**, offers no improvement over the simpler case **G1** or the C_1-symmetric **G4**. **G4** again asserts that a reduction of crowding or stereocenters does not imply a reduction in enantiodiscrimination.

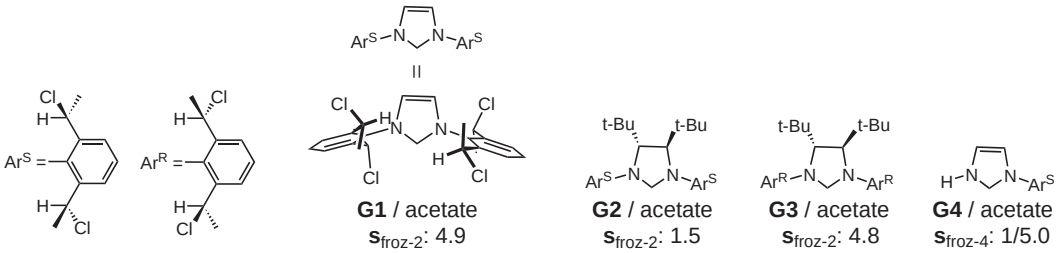

Figure 4.12: Carbene ligands with chirally modified N-aryl substituents.

Due to their unprecedented structure, type **G** ligands have not been extensively modeled, but

syntheses are known which leave stereocenters bound directly to the imidazole nitrogens (Figure 4.13). The relatively unencumbered ligands of type **H** offer good stability and reasonable activation barriers. Modest selectivities are predicted, though it is not obvious what effect the freely rotating N–C* bonds will have on the predictions' accuracy.

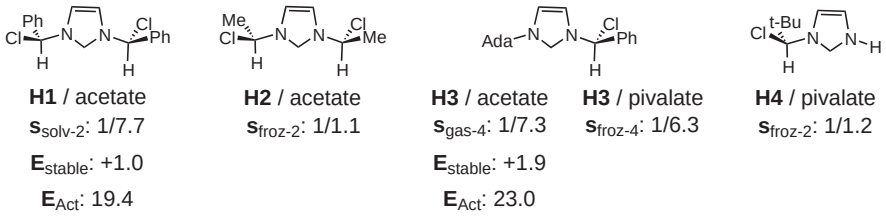

H1 / acetate
$s_{solv\text{-}2}$: 1/7.7
E_{stable}: +1.0
E_{Act}: 19.4

H2 / acetate
$s_{froz\text{-}2}$: 1/1.1

H3 / acetate
$s_{gas\text{-}4}$: 1/7.3
E_{stable}: +1.9
E_{Act}: 23.0

H3 / pivalate
$s_{froz\text{-}4}$: 1/6.3

H4 / pivalate
$s_{froz\text{-}2}$: 1/1.2

Figure 4.13: Carbene ligands with chiral N-alkyl substituents.

Placing stereocenters closer to the reaction center has led to moderate selectivity predictions, but the chiral groups investigated so far keep their stereogenic information constrained somewhat locally in space. As a result, *both* antipodean substrates tend to "get around" the ligands' chirality by finding at least one low-energy conformation of transition state TS3. For high selectivity to be observed, *all* the possible transition states incorporating one enantiomer must be at least 2 kcal/mol higher in free energy than the lowest transition state incorporating its antipode. Accordingly, we began to seek ligand structures with two characteristics. First, we sought to incorporate large, rigid fragments which (while not necessarily chiral themselves) would project the chirality of nearby stereocenters over a large volume of the reaction sphere. Second, any rotational degrees of freedom were to be damped as much as possible in order to discourage the ligand from relaxing to accomodate the chiral alcohols. The first generation of structures meeting these criteria offered encouraging results (Figure 4.14).

Ligands of type **I** incorporate the readily available 9H-fluoren-9-amine into the imidazole framework. (The building blocks 9-bromo- and 9-iodo-9H-fluorene are also available, which allows a synthetic route in which the fluorene fragment is appended to preformed chiral imidazoles, as in Figure 4.10.) As in ligands **B** through **F**, the t-butyl groups on the backbone hinder rotation of the N-substituents. However, the fluorene unit extends farther into the space around palladium

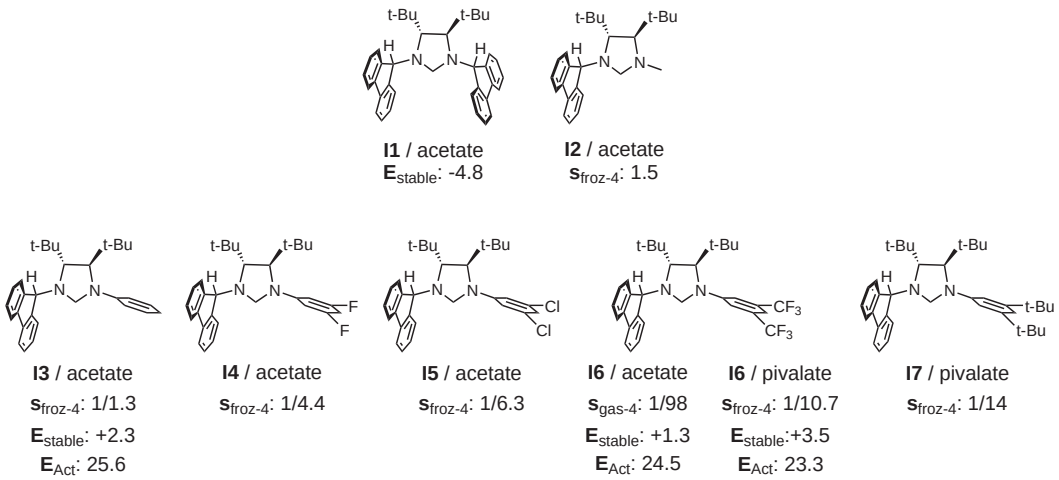

Figure 4.14: Carbene ligands with fluorene substituents.

than aryl derivatives. In fact the C_2-symmetric **I1** apparently forces too much crowding around the $Pd(OAc)_2$ fragment to be as stable as **A**. Stability could be regained by replacing one fluorene with a methyl (**I2**) or phenyl (**I3**) group. The selectivity predicted for **I3** is low because both of the (*S*)- and one of the (*R*)-diastereomers of TS3 have similar energies, while the second (*R*)-diastereomer lies about 2 kcal/mol higher. If the low-lying (*R*) state could be destabilized, selectivity would increase commensurately. We noticed an interaction unique to this (*R*) state; that the *meta*-hydrogen of the phenyl ring abutted the π-system of the substrate's phenyl ring. It was reasoned that increasing the size and electron-richness at this *meta* position would selectively destabilize the low-energy (*R*) state, and ligands **I3** through **I6** bear this out. This type of manipulation would not be possible without the geometric information provided by computational models. The decrease in activation energy upon addition of the trifluoromethyl group in **I6** is consistent with the stabilization of the Pd^0 product by the more electron-withdrawing ligand. Use of pivalate with **I6** further reduces the activation energy as expected by increasing the carboxylate's basicity.

The high predicted selectivity (1:98) of ligand **I6** leaves room to manipulate the catalyst parameters in order to balance activity, stability, and ease of synthesis. Many variations on the fluorene structure are available and if a C_2 analogue of **I1** with satisfactory properties can be identified, catalyst preparation may be simplified. The properties of ligands **I** offer proof-of-concept that a selective version of **A** can be identified, provided the racemization pathway discussed previously

can be avoided. We feel it unwise to proceed with further refinements of ligand structure until this issue can be soundly addressed experimentally. Future work should address the effects of solvation on selectivity and the relative thermodynamics of paths TS2 and TS3 in the most promising new ligands.

This section emphasizes what a small fraction of structures can be expected to fulfill several design criteria simultaneously. Experimental synthesis and testing of so many ligands would no doubt consume many times the man-hours of the computational screening. Of course, the cost of the theoretical approach is the time invested beforehand in determining how to screen.

4.3 On Asymmetric Ligands

The comparison of C_1- and C_2-symmetric ligands and their ability to induce enantioselectivity has been a recurring theme. One might argue that C_2 catalysts are more likely to be effective based on the combination of two points: that selectivity results from *all* of the diastereomeric transition states containing one enantiomer lying significantly higher in energy than the most favorable transition state of the other enantiomer, and that catalysts of higher symmetry will generate a smaller number of unique diastereomeric transition states. For example, a C_2-symmetric catalyst (like the bispidine complexes of chapter 3) may lead to only one unique transition state for each of two enantiomeric substrates. If energies within a realistic range of a few kcal/mol (we have seen it is not trivial to generate even this much dispersion among transition state energies) are assigned randomly to these two structures, there is some chance that the resulting energy difference will induce satisfactory selectivity. However, if a less symmetric catalyst is used (like the C_1 carbene ligands of this chapter), there may be two, three, or more unique transition state diastereomers for *each* enantiomer. If energies are randomly assigned to these structures from the same window of a few kcal/mol, the probability that all of one enantiomer's transition states remain significantly higher in energy than the other's is decreased.

The reasoning here, however, relies on transition state energies being randomly distributed. Modeling give us the ability to deliberately adapt a ligand structure to favor or penalize specific

interactions. Structures with no symmetry allow greater freedom to craft a ligand into an effective form. (When designing a C_2 ligand, one determines half the structure, and the other half is set by symmetry.) Since the substrates we seek to distinguish are typically C_1-symmetric fragments, it follows that a C_1-symmetric catalyst offers a better chance of fitting one enantiomer "like a glove." We note that the hypothesized carbene ligands with outstanding predicted selectivity were thoroughly asymmetric.

When the addition of solvation effects to gas phase selectivity predictions has had a significant effect, it has usually been positive. This was most dramatically (and experimentally) the case when the dielectric constant around the (–)-sparteine complexes in section 2.4 was increased to reflect vacuum, toluene, and chloroform. It also applies to ligand **I6** of the previous section[14]. This phenomenon can be rationalized in general by considering that the effect of a dielectric medium is to stabilize the separation of charge in a molecule by increasing dipole or higher multipole moments. The difference in energy between two diastereomeric transition states (Figure 4.15) can be caused by properly aligned and improperly aligned local poles found in the substrate and catalyst. As the solvent stabilizes these poles, the electrostatic interaction in the aligned case only becomes more favorable, while the improperly aligned case becomes more frustrated.

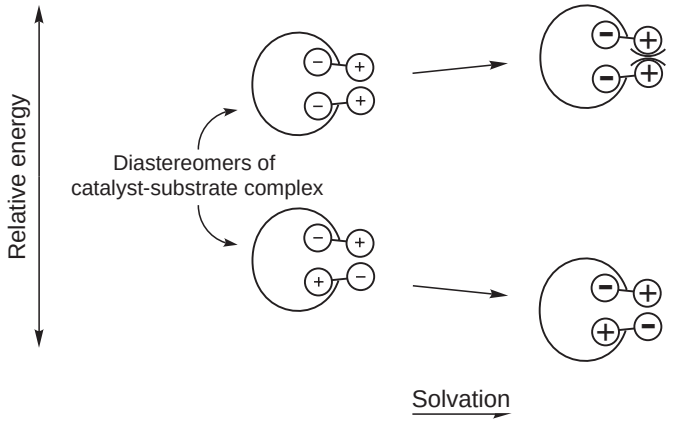

Figure 4.15: The effect of solvation on electrostatically-derived selectivity.

Future work should involve more in-solvent geometry optimizations of transititon states incorpo-

[14]Interestingly, the predicted selectivity of **F1** (in which selectivity is clearly derived from steric, not electrostatic, interactions) decreased slightly upon solvation.

rating the hypothesized carbene ligands in which electrostatic interactions were specifically intended to induce selectivity (**I4**–**I6**, **B3**).